

General and Domain-Specific Zero-shot Detection of Generated Images via Conditional Likelihood

Roy Betser^{1,2} Omer Hofman² Roman Vainshtein² Guy Gilboa¹
¹Technion - Israel Institute of Technology ²Fujitsu Research of Europe
 roy.betser@fujitsu.com

Abstract

The rapid advancement of generative models, particularly diffusion-based methods, has significantly improved the realism of synthetic images. As new generative models continuously emerge, detecting generated images remains a critical challenge. While fully supervised, and few-shot methods have been proposed, maintaining an updated dataset is time-consuming and challenging. Consequently, zero-shot methods have gained increasing attention in recent years. We find that existing zero-shot methods often struggle to adapt to specific image domains, such as artistic images, limiting their real-world applicability. In this work, we introduce CLIDE, a novel zero-shot detection method based on conditional likelihood approximation. Our approach computes likelihoods conditioned on real images, enabling adaptation across diverse image domains. We extensively evaluate CLIDE, demonstrating state-of-the-art performance on a large-scale general dataset and significantly outperform existing methods in domain-specific cases. These results demonstrate the robustness of our method and underscore the need of broad, domain-aware generalization for the AI-generated image detection task. Code is available at https://github.com/FujitsuResearch/domain_adaptive_image_detection.

1. Introduction

The rapid progression of generative methods, particularly diffusion models [23, 57], has made synthetic imagery remarkably realistic. These advancements boost creative and practical applications. However, they also pose significant risks in social media, journalism, and security, where manipulated imagery can facilitate misinformation, impersonation, and other forms of digital deception [58, 71]. Hence, the development of reliable detection methods is crucial to preserving public trust and ensuring digital integrity.

Prior research on generated image detection includes classification-based and semi-supervised approaches [5, 8,

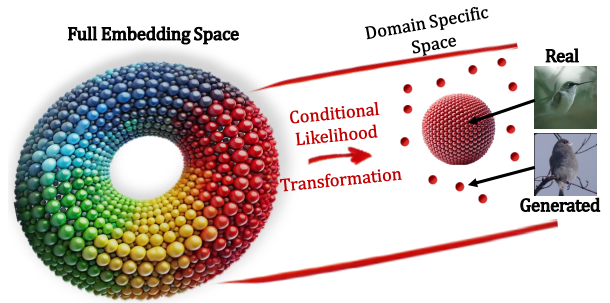


Figure 1. **Conditional likelihood illustration.** Our adaptive image detection method. When conditioned by real images from a specific domain (red dots), generated images become unlikely.

17, 59]. The performance of these methods heavily depends on the quality and diversity of the training data, which includes both synthetic and real images [25]. However, as novel generative models continue to emerge at a rapid pace, maintaining an updated synthetic training set becomes not only impractical but sometimes impossible. This is especially true in misinformation campaigns orchestrated by actors who may develop or access entirely new generation techniques. This highlights the need for detection frameworks that can adapt to unseen generative techniques without relying on new data from every new model.

Zero-shot learning is well-suited for generated image detection as it eliminates the need for large training datasets, prior knowledge of generative models, or continual monitoring of new techniques. In this context, as established in [12, 19, 33, 63], zero-shot means distinguishing between real and generated images without any exposure to generated content or task-specific training. While this line of work has enabled promising progress, existing zero-shot methods still exhibit limited robustness and sharp performance swings across generators [12].

To meet real-world needs, we formalize *domain-specific zero-shot detection*: operate within a narrow target domain using only a set of *real* domain image, with no access to generated samples and no task training (see Supp. Sec. I)

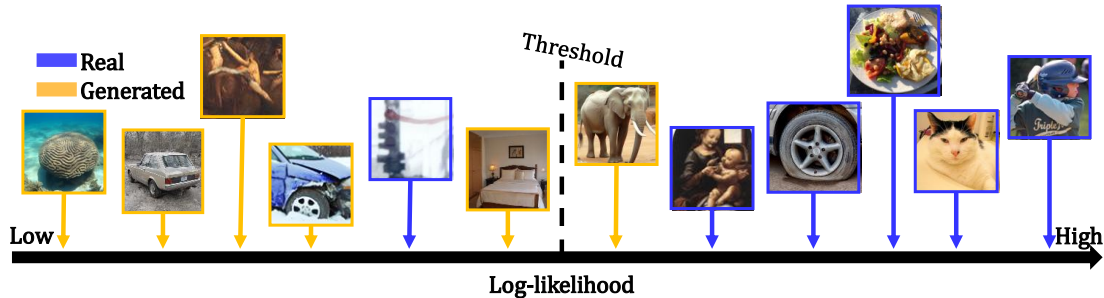


Figure 2. **General real and generated images.** Real and generated images of general real-world imagery. A blurred real image is misclassified as generated. A realistic generated image of an elephant is misclassified as real. All other examples are correctly classified.

for task definition and discussion). This setting, analogous to cross-task robustness in LLM-generated text detection [78], reveals severe failures of existing image detectors on narrow domains. We introduce two practical benchmarks (damaged cars, invoices) and show that CLIDE sustains high accuracy where prior methods degrade.

Our fundamental premise is that foundation models, trained on huge datasets of real images, capture well the subtle attributes differentiating real images from generated ones. However, accessing likelihood in such black-box models is a very complex task, and more broadly, computing likelihoods for images is a challenging task in computer vision [26, 42]. Current computer vision models primarily rely on likelihood gradients or score functions, which constrain direct likelihood computation [35]. A recent study [7] proposed a simple method to estimate image likelihood based on Contrastive Language-Image Pre-training (CLIP) [60]. CLIP is a foundation model that is widely used across various computer vision tasks [17, 50]. We generalize this approach by introducing a conditional likelihood framework that enables domain adaptation and strengthens robustness for zero-shot generated image detection.

Our main contributions are:

1. We introduce a conditional likelihood approximation model for images based on CLIP embeddings, and show how the model can be validated through statistical tests.
2. We propose CLIDE, a zero-shot generated image detection method applicable to both general images (Fig. 2) and domain-specific images (Fig. 1). CLIDE significantly outperforms four state-of-the-art zero-shot detection baselines on a large-scale general image dataset.
3. We demonstrate the domain adaptation capabilities of CLIDE on three specific domains: artistic images, damaged car images and invoice document images. Our method consistently maintains high performance, while other methods experience a decrease in effectiveness in domain-specific content.
4. We present two new synthetic datasets of damaged cars (6K images) and invoice images (3K).

2. Background and Related Work

Generated image detection. Early work on detecting AI-generated images predominantly employed supervised methods, often training standard CNNs to distinguish real and generated images [5, 8, 25, 72]. Subsequent studies refined these methods by focusing on key phenomenological cues to enhance separability [4, 15, 47, 69, 74, 83]. However, they largely relied on comprehensive datasets from known generative models, limiting their ability to manage newly emerging generative techniques [52].

To address the need for broader generalization, unsupervised and semi-supervised techniques were explored [17, 59, 81, 82], yet these methods required partial knowledge of the generative processes during training. Additional works [18, 52, 67] leverage feature representations from large pre-trained models to enhance performance in data-limited settings. Still, some reliance on generated data or familiarity with generative techniques persists.

Zero-shot detection strategies aim to identify generated images without prior exposure to any particular generative models or synthetic datasets. Existing zero-shot detection methods typically analyze an image’s robustness to a specific transformation (*e.g.* denoising, compression), and compare the original and transformed images to assess authenticity. AEROBLADE [63] employs a pre-trained auto-encoder, using its reconstruction error as a detection criterion, while RIGID [33] evaluates the similarity between an image and its noise-perturbed counterpart. Other approaches explore alternative transformations: ZED [19] estimates pixel-wise probability distributions via lossless encoding; Manifold-Bias [12] uses a diffusion model and CLIP to compute differential measures in the learned probability space.

While effective in a general setting, these approaches implicitly rely on approximate probability functions that can be unstable and sensitive to variations in generative models. Moreover, as shown in our experiments, their performance degrades significantly in domain-specific scenarios, highlighting a key shortcoming in generalization across real-

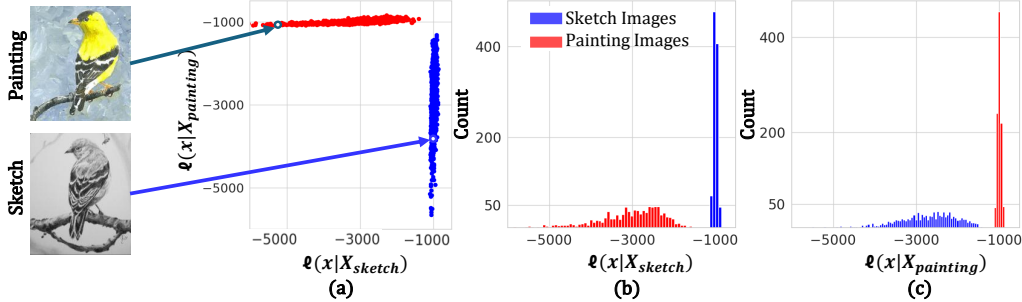


Figure 3. **Conditional likelihood across domains.** Despite semantic similarity, “sketch” and “painting” images from ImageNet-R yield separable distributions under our log-likelihood approximation. (a) 2D scatter plot of likelihoods conditioned on each domain. (b, c) Histograms show that each domain assigns higher likelihoods to its own images, with lower and more variable scores for the other.

world image distributions. In contrast, our method explicitly models the distribution of real images and offers inherent flexibility to adapt across domains, resulting in a more robust and versatile zero-shot detection solution.

Likelihood approximation for images. Estimating the likelihood of images is a fundamental problem with wide-ranging applications in computer vision [24, 30, 44, 70, 80]. The likelihood of an image refers to the probability density function that describes how probable a given image is under a learned or assumed distribution of natural images. The early methods relied on assumptions about the smoothness of natural images [28] and the statistical distribution of image patches [86]. The advent of generative models, including GANs [29] and Diffusion Models [68], has significantly improved image synthesis by learning implicit representations of the likelihood. However, these models do not provide direct access to the likelihood function itself. Recently, [7] proposed leveraging CLIP [60] to obtain a likelihood approximation through the whitening transform. Following this, we introduce a conditional likelihood approximation and apply it to the task of generated image detection.

3. Conditional Likelihood Approximation

We follow [7], which introduced the use of whitened CLIP (W-CLIP) for likelihood estimation. Here, we extend this general likelihood estimation framework to a conditional likelihood estimation.

3.1. Global CLIP likelihood (recap)

Notations: Let $\mathcal{X} = \{x_1, \dots, x_N\}$ be N vectors in \mathbb{R}^d , and let $\mathbf{X} \in \mathbb{R}^{d \times N}$ denote their column-stacked matrix, with mean $\mu = \frac{1}{N} \sum_{i=1}^N x_i$. The centered vectors are $\hat{x}_i = x_i - \mu$, and let $\hat{\mathbf{X}} \in \mathbb{R}^{d \times N}$ be the column-stacked matrix of centered vectors. The empirical covariance matrix is $\Sigma = \frac{1}{N} \hat{\mathbf{X}} \hat{\mathbf{X}}^\top$.

Whitening Transform: We compute a whitening matrix $W \in \mathbb{R}^{d \times d}$ satisfying $W^\top W = \Sigma^{-1}$. Using PCA, we diagonalize Σ as $\Sigma = V \Lambda V^\top$, where Λ contains eigenval-

ues and V contains eigenvectors. The whitening matrix is $W = \Lambda^{-\frac{1}{2}} V^\top$. A vector x is whitened via $y = W \hat{x}$, and the whitened matrix is $\mathbf{Y} = W \hat{\mathbf{X}}$. The whitened vectors are isotropic with zero mean and identity covariance.

Likelihood Approximation: Prior work suggests CLIP’s image and text latent spaces are approximately disjoint [43, 45], allowing each modality to be modeled independently. When whitening statistics are estimated on a broad real-image corpus (e.g., MS-COCO val), the whitened CLIP embeddings have identity covariance by construction; empirical tests on MS-COCO (Anderson–Darling [1], D’Agostino–Pearson [20]) further indicate that the whitened coordinates are approximately i.i.d. standard normal. The log-likelihood of a whitened vector y is:

$$\ell(y) = -\frac{1}{2} (d \log(2\pi) + |y|^2), \quad (1)$$

where $|y|^2 = y^\top y$. Given an embedding x , the whitened vector $y = W \hat{x}$ provides a direct likelihood approximation.

Global likelihood gap. Contrastive training pulls semantically similar images together and pushes dissimilar ones apart along *directions* in the embedding space [65]. The score in Eq. (1), however, depends only on the squared norm $\|W \hat{x}\|^2$, discarding directional information. As a result, distinct domains that occupy different subspaces but lie at comparable radii from the origin can appear similarly likely under a *global* surrogate. This motivates conditioning the covariance on domain evidence to assess domain-relevant directional structure.

3.2. Conditional likelihood

Building on the global likelihood model, we formulate a *family of domain-conditional* likelihoods by estimating whitening on domain-specific data and scoring within the domain’s dominant subspace. We also verify approximate normality on small ($\sim 1K$) domain sets, empirically justifying the conditional likelihood estimation.

Theory. Let the global likelihood follow Eq. (1), and

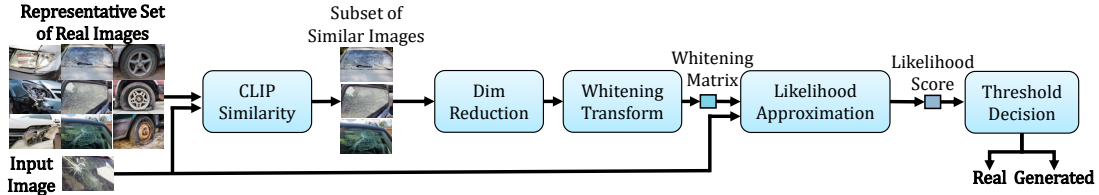


Figure 4. **Method flowchart.** The input image is embedded using CLIP, followed by a selection of a subset k of similar image embeddings from the representative set (X). A whitening matrix (W), with reduced dimensions (m), is computed using this subset (X_k). The whitening matrix is then applied to calculate a likelihood score (Eq. (2)). The final decision is determined based on an empirical threshold.

let $y(j)$ denote the j -th coordinate of a whitened vector $y \in \mathbb{R}^d$. Conditioning on a linear constraint (e.g., $y(j) = c$) reduces the effective dimension by one and yields a standard normal on a $d - 1$ dimensional subspace; more generally, conditioning on l independent constraints restricts the support to a $(d-l)$ -dimensional subspace with standard normal coordinates on that subspace. In practice, domain evidence induces *low variance* along some directions; estimating the covariance on domain-specific data and restricting to the top- m eigenvectors (with $m \leq d$) recovers an isotropic model on the domain’s dominant subspace.

Domain taxonomy. Each image can belong to multiple, possibly overlapping *domains*, i.e., sets of images sharing characteristics (e.g., an image of a yellow bus in a city belongs to real-world, transportation, color, and urban domains).

Model. Given a domain \mathcal{D} occupies an (unknown) subspace of $m = d - l$ dominant dimensions, with the remaining l directions exhibiting low variance. Given domain evidence $X = \{x_i\} \subset \mathcal{D}$, we compute the conditional whitening matrix $W(X, m) \in \mathbb{R}^{m \times d}$ using the top- m eigenvectors. The conditional log-likelihood is then:

$$\ell(x | X, m) = -\frac{1}{2} \left(m \log(2\pi) + \|W(X, m) \hat{x}\|^2 \right). \quad (2)$$

Empirical validation. A necessary precondition for conditional likelihood is that, after whitening on domain-specific evidence, coordinates are approximately Gaussian on the domain’s dominant subspace. We validate this on small ($\sim 1\text{K}$) ImageNet-R [34] domains (*sketch*, *painting*): normality tests on whitened coordinates pass clearly (Supp. Sec. B), and cross-domain (e.g., W_{sketch} applied to *painting* and vice versa) preserves acceptable Gaussianity while inducing systematic likelihood shifts. As shown in Fig. 3, the 2D scatter and 1D histograms exhibit clear cross-domain separation, demonstrating robust distributional distinctions even between semantically similar images. As shown in Supp. Sec. B, Fig. 3b, retaining all d dimensions yields substantial inter-coordinate correlations, violating the isotropic/i.i.d. assumption underlying Eq. (2).

Consequently, restricting the whitened space to a lower-dimensional subspace (top- m components) is essential.

Conditional vs. global. Whereas W-CLIP estimates a single *global* surrogate on a broad real-image corpus, our formulation provides a *family of domain-conditional* likelihoods by using data limited to a specific domain. This shift is conceptually distinct and empirically necessary to avoid global-surrogate failure modes, and it directly enables our zero-shot detector (Sec. 4). Statistical checks (Supp. Sec B) and a side-by-side comparison of global vs. conditional models and performance are provided in Supp. Sec J.

4. Method: CLIDE

We introduce **CLIDE** (Conditional Likelihood generated Image DEtector), a zero-shot generated image detection method based on the proposed conditional likelihood approximation, conditioning on *real images* to distinguish generated content. An overview is given in Fig. 4 and in the high-level Algorithm 1. A detailed algorithm is in Supp. Sec. A. In the following, we outline the key components of our approach.

Algorithm 1 CLIDE - high level

Inputs: I (input image), X (reference set), k (neighbors), m (components), th (threshold)

Outputs: Likelihood score $\ell(I | X, k, m)$, label C

- 1: **Step 1:** Embed the input image to obtain x , and compute cosine similarities with the embeddings in $X^{d \times N}$.
 - 2: **Step 2:** Select the top- k most similar embeddings - X_k .
 - 3: **Step 3:** Compute mean vector $\mu(X_k)$ and whitening matrix $W(X_k, m)$ using top- m eigenvectors.
 - 4: **Step 4:** Compute likelihood $\ell(I | X, k, m)$ and compare to threshold th to assign label C .
-

Motivation. CLIP embeddings encode semantic information [60], which can bias likelihood estimates. For example, zebras tend to have higher likelihoods than plates of food, making a generated zebra potentially more likely than a real plate (Supp. Sec. C, Fig. 4). CLIP also captures domain-specific traits, as shown in Fig. 3, where conditioning shifts

Generative Model	AEROBLADE [63]				RIGID [33]				ZED [19]				Manifold Bias [12]				CLIDE (ours)			
	AUC ↑	AP ↑	F1 ↑	Acc ↑	AUC ↑	AP ↑	F1 ↑	Acc ↑	AUC ↑	AP ↑	F1 ↑	Acc ↑	AUC ↑	AP ↑	F1 ↑	Acc ↑	AUC ↑	AP ↑	F1 ↑	Acc ↑
ProGan [38]	0.54	0.49	0.65	0.54	0.45	0.46	0.16	0.48	0.74	0.75	0.7	0.64	0.96	0.97	0.88	0.88	0.95	0.96	0.87	0.88
StyleGan [39]	0.58	0.59	0.63	0.51	0.71	0.72	0.56	0.65	0.75	0.77	0.71	0.65	0.68	0.74	0.61	0.68	0.76	0.71	0.75	0.73
StyleGan2 [40]	0.74	0.76	0.68	0.61	0.52	0.54	0.31	0.53	0.75	0.8	0.68	0.61	0.62	0.66	0.48	0.6	0.8	0.82	0.73	0.68
BigGAN [10]	0.65	0.61	0.68	0.6	0.62	0.63	0.42	0.57	0.45	0.47	0.63	0.5	0.9	0.9	0.8	0.81	0.96	0.96	0.87	0.88
GauGan [55]	0.7	0.71	0.68	0.6	0.32	0.39	0.1	0.45	0.33	0.41	0.6	0.44	0.98	0.98	0.91	0.9	0.83	0.85	0.76	0.73
CycleGan [84]	0.76	0.73	0.73	0.69	0.34	0.39	0.05	0.43	0.22	0.38	0.6	0.43	0.97	0.97	0.89	0.9	0.98	0.98	0.9	0.91
CRN [16]	0.34	0.51	0.48	0.59	0.25	0.36	0.01	0.42	0.99	0.99	0.92	0.92	0.93	0.9	0.88	0.88	0.98	0.99	0.91	0.92
SD V1.4 [64]	0.47	0.47	0.63	0.51	0.79	0.77	0.63	0.69	0.62	0.65	0.65	0.54	0.71	0.62	0.4	0.57	0.9	0.91	0.82	0.82
SD V1.5 [64]	0.49	0.49	0.64	0.52	0.77	0.76	0.63	0.68	0.61	0.63	0.65	0.54	0.72	0.64	0.44	0.58	0.9	0.91	0.83	0.82
Guided DM [23]	0.55	0.49	0.66	0.57	0.51	0.51	0.25	0.5	0.58	0.55	0.68	0.59	0.8	0.8	0.66	0.7	0.87	0.87	0.79	0.78
LDM 100 [64]	0.48	0.48	0.62	0.48	0.51	0.51	0.25	0.5	0.52	0.56	0.63	0.49	0.84	0.88	0.78	0.79	0.92	0.93	0.84	0.85
LDM 200 [64]	0.47	0.48	0.62	0.48	0.51	0.51	0.25	0.5	0.53	0.56	0.63	0.5	0.85	0.88	0.79	0.8	0.92	0.93	0.85	0.85
Glide 50 27 [51]	0.06	0.32	0.59	0.42	0.51	0.51	0.25	0.5	0.98	0.98	0.91	0.92	0.93	0.94	0.86	0.86	0.91	0.92	0.84	0.84
Glide 100 27 [51]	0.08	0.32	0.6	0.43	0.51	0.51	0.25	0.5	0.98	0.98	0.91	0.92	0.92	0.93	0.84	0.84	0.91	0.92	0.83	0.83
Glide 100 10 [51]	0.04	0.31	0.59	0.42	0.51	0.51	0.25	0.5	0.98	0.98	0.92	0.92	0.93	0.93	0.85	0.85	0.91	0.92	0.83	0.83
ADM [23]	0.45	0.43	0.65	0.56	0.56	0.57	0.39	0.56	0.47	0.46	0.65	0.55	0.62	0.57	0.32	0.53	0.89	0.88	0.84	0.84
DALL-E 3 [6]	0.35	0.41	0.61	0.45	0.51	0.51	0.25	0.5	0.45	0.5	0.62	0.47	0.82	0.84	0.71	0.74	0.96	0.96	0.88	0.89
Midjourney [48]	0.29	0.37	0.6	0.43	0.65	0.66	0.48	0.6	0.92	0.93	0.84	0.84	0.56	0.53	0.27	0.51	0.9	0.84	0.85	0.85
VDQM [31]	0.51	0.47	0.66	0.57	0.53	0.54	0.32	0.53	0.46	0.46	0.63	0.49	0.83	0.83	0.7	0.73	0.92	0.93	0.84	0.84
Wukong [49]	0.48	0.47	0.62	0.49	0.63	0.6	0.37	0.55	0.39	0.45	0.6	0.44	0.73	0.69	0.5	0.62	0.95	0.96	0.88	0.88
All	0.52	0.48	0.64	0.53	0.51	0.53	0.28	0.52	0.69	0.66	0.69	0.62	0.85	0.88	0.76	0.78	0.91	0.91	0.84	0.84

Table 1. **Evaluation of detection on general images.** Our method achieves the highest overall performance across all models combined and outperforms competing methods on most generative models. The best result for each metric in each row is highlighted in bold.

the distribution of similar images (*e.g.* birds on branches) across domains. To improve detection, we aim to minimize semantic bias while enhancing domain-specific separation.

Whitening Data Selection. Distinguishing real from high-quality generated images is subtle. We address this with adaptive whitening. Given a set X of real images, we select the k most similar images to the input based on cosine similarity of CLIP embeddings. The whitening matrix is computed using this subset, $W(X_k, m)$, enabling the conditioned likelihood to adapt to the local semantic subspace.

Dimensionality Reduction. Conditioned likelihood operates in a subspace of the embedding space (Sec. 3.2), defined by the selected samples for whitening. Additionally, when using a small number of samples for whitening, some eigenvalues approach zero, causing instability. Dimensionality reduction mitigates these issues and enhances both performance and efficiency (Supp. Sect. B, E, Figs. 3, 6).

Domain-adaptation. Our method can target a specific domain and distinguish real from generated content within it. As in general domain adaptation methods, a small set of images from the target domain is needed to support detection. This set serves as the representative set X for conditional likelihood estimation. In Sec. 5.3, we examine the method’s robustness to different choices of X , showing many real-world datasets yield similar results in the general case. For domain specific detection, target samples must be included in X , but do not need to dominate it; mixed domain sets still support high detection performance across domains.

By integrating these steps into the computation of the likelihood score, we can directly utilize it as a differentiation criterion between real and generated images. Our method has unique characteristics distinguishing it compared to existing zero-shot detection methods:

- **Real image likelihood.** First method utilizing a likelihood estimation for the generated image detection task.
- **Domain adaptability.** Using sample images for the conditional likelihood enables a domain-adaptive approach.
- **Explicit probabilistic computation.** Other methods implicitly try to find a probabilistic differentiation between real and generated images. Our method explicitly computes the probabilities, yielding a stable distinction.

5. Evaluation

We evaluate in two setups. First, a *general* setting using a diverse image benchmark to assess detection ability and compare against leading zero-shot methods. Second, we introduce a *domain-specific detection* task that targets three concrete domains-artistic images, damaged cars, and invoice documents. Both real and generated content come from a narrow distribution. This setting is underexplored yet practically critical (*e.g.*, fraud detection). Across these domains, *all* existing zero-shot detectors degrade sharply (often with $AUC < 0.6$ and flipped decisions; see Tabs. 2 and Fig. 5), whereas our conditional likelihood maintains high accuracy ($AUC \gtrsim 0.9$). We additionally provide the first synthetic benchmarks for damaged cars and invoices. This dual evaluation highlights both standard zero-shot performance and, crucially, CLIDE’s unique strength in domain-adaptive detection.

Implementation Details. We set $k = 500$ and $m = 400$ (real samples for whitening and dimensions) across all domains (see Sec. 5.3 for details). We use the CLIP ViT-L/14 model [60]. Our full code is provided in the Supplementary Material. For AEROBLADE and Manifold Bias, we use official implementations. As no official code exists for RIGID and ZED, we self-implement them. For RIGID, we

Generative Model	AEROBLADE [63]				RIGID [33]				ZED [19]				Manifold Bias [12]				CLIDE (ours)			
	AUC ↑	AP ↑	F1 ↑	Acc ↑	AUC ↑	AP ↑	F1 ↑	Acc ↑	AUC ↑	AP ↑	F1 ↑	Acc ↑	AUC ↑	AP ↑	F1 ↑	Acc ↑	AUC ↑	AP ↑	F1 ↑	Acc ↑
Artistic Image Domain																				
StyleGan3 [41]	0.81	0.84	0.72	0.69	0.32	0.39	0.06	0.46	0.38	0.41	0.63	0.5	0.96	0.96	0.9	0.9	0.98	0.99	0.93	0.93
SD2.1 [64]	0.57	0.6	0.61	0.48	0.77	0.75	0.52	0.64	0.17	0.34	0.61	0.44	0.91	0.9	0.83	0.84	0.98	0.98	0.92	0.93
SDXL [57]	0.62	0.69	0.6	0.46	0.64	0.6	0.3	0.54	0.33	0.43	0.61	0.44	0.83	0.81	0.71	0.75	0.97	0.98	0.91	0.91
AniImagineXL [46]	0.66	0.75	0.6	0.47	0.39	0.42	0.08	0.46	0.45	0.59	0.61	0.44	0.28	0.37	0.02	0.44	0.76	0.83	0.66	0.55
All	0.65	0.7	0.62	0.52	0.53	0.55	0.26	0.53	0.33	0.41	0.61	0.45	0.74	0.8	0.69	0.73	0.92	0.92	0.83	0.82
Damaged cars Image Domain																				
Kandinsky2.1 [62]	0.29	0.38	0.6	0.43	0.3	0.38	0.06	0.44	0.68	0.66	0.68	0.61	0.6	0.64	0.48	0.61	0.97	0.98	0.93	0.93
SDXL [57]	0.34	0.4	0.61	0.45	0.3	0.38	0.06	0.44	0.83	0.85	0.76	0.73	0.32	0.42	0.15	0.49	0.97	0.97	0.91	0.91
DALL-E 3 [6]	0.39	0.45	0.6	0.44	0.4	0.42	0.11	0.42	0.15	0.33	0.59	0.42	0.14	0.33	0.03	0.44	0.99	0.99	0.93	0.93
Midjourney [48]	0.46	0.47	0.62	0.47	0.51	0.5	0.23	0.5	0.78	0.75	0.74	0.71	0.4	0.44	0.13	0.48	0.93	0.94	0.87	0.86
UnCLIP [61]	0.22	0.35	0.6	0.43	0.69	0.67	0.46	0.6	0.31	0.38	0.61	0.46	0.69	0.68	0.48	0.61	0.8	0.8	0.72	0.67
All	0.33	0.4	0.61	0.44	0.45	0.48	0.21	0.49	0.61	0.54	0.68	0.61	0.47	0.53	0.3	0.53	0.92	0.92	0.85	0.84
Invoice Image Domain																				
GPT-Image-1 [53]	0.53	0.62	0.56	0.47	0.57	0.67	0.12	0.53	0.6	0.56	0.65	0.54	0.61	0.58	0.55	0.62	0.91	0.92	0.82	0.82

Table 2. **Detection performance on domain-specific images.** Our method consistently maintains high performance, while others show significant drops. It outperforms all baselines across all three domains - both per model and when tested on all models combined - using a single model for the invoice domain due to the lack of other high-quality sources. Best results per row are in bold.

use the DINO model [14]; for ZED, we apply the lossless compression method SRc [13]. ZED proposes four criteria; we report the best-performing one in the general image domain (D_0). Results for the other criteria are provided in Supp. Sec. H, Tabs. 2 and 3.

Metrics. We evaluate each detection method using four metrics. To measure the separation between real and generated image distributions, we use two standard metrics: Area Under the Curve (AUC) and Average Precision (AP). Classification performance is further assessed using F1 score and accuracy. The binary classification threshold is set for all methods as $th = \text{mean}(C_{th}) + \text{std}(C_{th})$, where C_{th} are the criterion values of a set of real images.

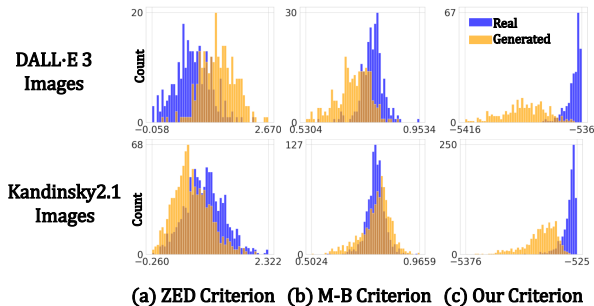


Figure 5. **Inconsistent separation direction - “flipped classification”.** ZED (a) and Manifold Bias (b) show inconsistent behavior across generative models, with real and generated scores flipping. Our method (c) yields consistent results, assigning higher likelihoods to real images. Example from the damaged cars domain.

5.1. General image detection

Dataset. In the general image domain, we follow [12] and combine three large-scale datasets [52, 72, 85], containing 100K generated images from GANs, diffusion models, and

commercial tools. A full list of the 20 generative models is provided in Tab. 1. We use the real images from [52, 72], originally sourced from LAION [66]. As there are only 50K real images from LAION, we sample an additional 50K from the MS-COCO training set to form the 100K real subset used in the “all” row of Tab. 1, totaling 200K images for evaluation. Each generative model contributes at least 1K generated samples, which are evaluated against an equal number of randomly selected real images from LAION, consistently applied across all detection methods. Following [7], we use 5K MS-COCO validation images for threshold calibration for all methods, and as the representative set for our method. An ablation appears in Sec. 5.3.

Results. The last row in Tab. 1 shows that our method outperforms all other zero-shot detection approaches. Our method also achieves the best results per generative model in most cases. While ZED or Manifold Bias surpass our approach for certain models, our results remain competitive. Notably, our proposed method consistently yields high performance across all models, with AUC dropping below 0.8 only for StyleGAN (0.76). In contrast, all other detection methods exhibit AUC values below 0.6 for certain generative models. We recall that an AUC below 0.5 indicates a complete failure for binary classification, where generated images are more likely to be classified as real ones. We refer to this phenomenon as “flipped classification” and illustrate it in Fig. 5. Since detection methods aim to maintain robustness across multiple models, this presents a significant limitation.

5.2. Domain specific detection

While our method performs well in general image detection, its key advantage is adaptability to new domains. To demonstrate this, we evaluate all methods across three spe-

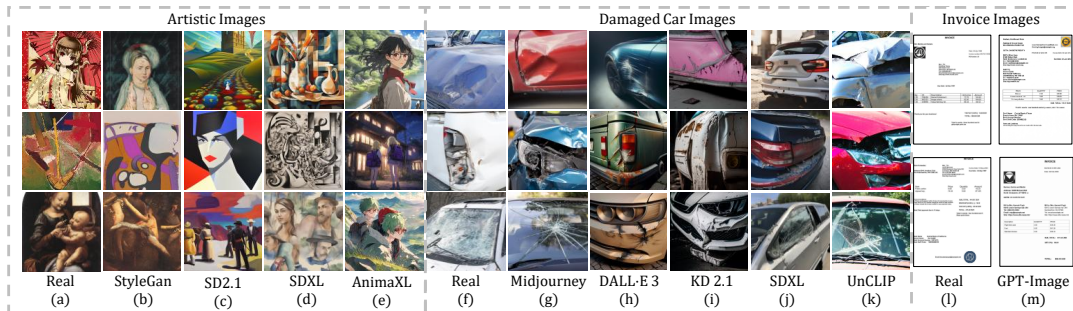


Figure 6. **Example images.** Examples of real images (a [2, 77], f [73], m [76]) and images generated using different generative models from different domains. Artistic generated images (b-e) are taken from [9] and all other generated images are generated by us.

cific domains. Existing approaches can only use domain-specific data for threshold calibration, whereas our method also leverages it for likelihood estimation. In each domain, we assume access to 1K real images (separate from the test set), used by all methods for calibration. Our method also uses them as the representative set.

Artistic image domain. The generation of images in specific artistic styles is a well-studied area in image synthesis and style transfer [11, 27, 37, 75]. Given the diversity of artistic styles across different artists, this is a broad and varied domain of images. We use images from ImagiNet [9], a real and generated artistic image dataset. Synthetic images are generated using four different generative models (see Tab. 2). Examples of real and generated images are shown in Fig. 6. Detection results for all methods are summarized in Tab. 2. In this domain, AnimaginXL [46] presents the most challenging generative model, as it is specifically fine-tuned for generating images in a distinct artistic style (Anime). Our method outperforms all detection approaches across all generative models and in the combined evaluation (“all”). Furthermore, unlike competing methods, our performance remains consistent with the general image case (Tab. 1), whereas the strongest competitors in the general image domain ([19], [12]) exhibit a decline in performance.

Damaged car image domain. Damaged car images form a niche but highly practical domain, relevant to insurance, rental, and second-hand vehicle markets [73]. Prior work has focused on damage detection and classification [32, 54, 56], but progress has been hindered by the lack of public benchmarks, with early studies relying on private datasets. CarDD [73] addressed this by releasing 4K real damaged car images; We use the training set (2,816 images) for evaluation and sample 1K calibration images from the validation and test splits. As no synthetic dataset exists for this domain, we generate the *first publicly available set of synthetic damaged car images* (see Fig. 6). The data is produced using two diffusion models, two commercial tools, and UnCLIP [61], which is conditioned on real images to

enhance realism and detection difficulty. Additional dataset details and samples are in Supp. Sec. F.1; the full dataset will be released upon acceptance. Our method maintains high performance in this domain, comparable to results in general and artistic domains, while other methods degrade (see Tab. 2). A key issue is flipped classification (Fig. 5), where ZED and Manifold Bias often misclassify generated images as real. In contrast, our method remains stable, consistently achieving AUC scores above 0.5 across all models. While ZED performs well on some models, its overall zero-shot reliability is limited by this failure mode.

Rep. Set Composition	LAION	MS-COCO	Flickr	Combined
MS-COCO	0.92	0.92	0.89	0.91
LAION	0.9	0.86	0.85	0.87
Flickr8k	0.89	0.88	0.95	0.9
ImageNet	0.73	0.75	0.77	0.75
MS-COCO + Flickr8k	0.91	0.92	0.93	0.93
LAION + ImageNet	0.86	0.82	0.83	0.83
All Sources Combined	0.92	0.92	0.92	0.91

Table 3. **Real data sources.** AUC values. Different representative set sources and test set sources of real images.

Invoice image domain Invoice images form a critical domain, particularly relevant to financial institutions, e-commerce platforms, and document verification systems. While prior work has focused on information extraction and document classification [3, 22, 79], little attention has been given to the detection of synthetically generated invoices. Existing datasets typically contain only real invoices, with no public benchmark for synthetic invoice detection. The generation of high-quality, text-rich invoice images was not feasible until the recent release of the GPT-Image-1 model [53], which enables the creation of visually and semantically realistic document images. For this study, we use real invoices from [76], selecting 3K images for evaluation and another 1K for calibration. Synthetic images are generated using GPT-Image-1, each conditioned on a corresponding test image with slight random variations in elements such

as price, product name, or date. We rely exclusively on GPT-Image-1, as it is currently the only model capable of producing high-quality document images for this task (see examples with other models in Supp. Sec. F.2, Fig. 14). Examples of real and generated invoices are shown in Fig. 6, and additional details are provided in Supp. Sec. F.2. Our method demonstrates high detection performance in this domain, while other methods suffer significant performance drops (see Tab. 2). These results highlight the importance of domain adaptability and the limitations of existing zero-shot detection methods in complex domains.

5.3. Robustness and efficiency analysis

Representative set. We study the impact of the representative set’s composition in both settings: general and domain-specific image detection.

General detection. We evaluate four real-world image sources as representative sets: MS-COCO (5K images), LAION (10K, from [72]), Flickr8k [36] (8K), ImageNet [21] (50K), and their combinations. Evaluation is performed on four fixed test sets from different sources, each containing 10K real and 10K generated images (except Flickr, with 3K each). As shown in Tab. 3, our method consistently achieves high AUC across all sources, except for ImageNet (0.73), likely due to its object-centric nature.

Domain-specific detection. We evaluate three domains (Cars, Art, Invoices), using 2K real and 2K generated images per domain, along with the general domain (10K each). We compare three representative set types: general-only, domain-only (1K images), and combined. As shown in Tab. 4, general-only sets yield lower AUC scores on specific domains, while adding just 1K domain-specific samples raises AUC to 0.91–0.94. Combining general and domain-specific sources further improves robustness across domains. Notably, multi-domain representative sets achieve $AUC > 0.9$ for all domains and maintain strong general-domain performance. These results demonstrate that our method is robust to representative set composition and adapts well to new domains with minimal supervision.

Rep. Set Composition	General	Damaged Cars	Artistic	Invoice
General only	0.92	0.56	0.77	0.34
Cars Only	0.53	0.93	0.57	0.8
Art Only	0.82	0.55	0.94	0.27
Invoice Only	0.55	0.69	0.6	0.91
General + Cars	0.9	0.93	0.62	0.8
General + Invoice	0.92	0.56	0.79	0.91
Cars + Art + Invoice	0.8	0.93	0.95	0.91
All Domains Combined	0.9	0.93	0.93	0.91

Table 4. **Representative set domain combinations.** AUC scores. Adding domain-specific samples improves in-domain performance; combined sets perform well across all domains.

Parameter Ablation study. We conduct ablation studies to evaluate the impact of the parameters in our method.

We analyze the effect of the number of whitening dimensions (m) and samples (k), finding optimal values around $m = 300-400$ and $k = m + 100$. We also compare global and per-image (local) whitening matrices, finding that local sampling yields slightly better performance, while the global setting offers improved efficiency with minimal loss. Overall, the method is robust to parameter selection, results are shown in Supp. Sec. E, Figs. 6–8.

Robustness to image perturbations. We assess the robustness of our method under common image degradations, including JPEG compression, Gaussian blur, random resizing and cropping, noise injection, and color jittering. Perturbations are applied only to inference images, with the representative set kept unchanged, isolating robustness to input variation. Results (Supp. Sec. E.2, Figs. 9–11) show that our method maintains high accuracy ($AUC > 0.8$) across all perturbations. Only under extreme distortions - such as noise with $\text{std} = 0.5$ or JPEG quality = 1% - does performance drop below 0.8 AUC.

Efficiency Analysis. Our method operates efficiently, achieving inference speeds comparable to ZED (0.25 seconds per image), while other methods, particularly AER-OBLADE, exhibit significantly higher latency (>4 seconds per image; see Supp. Sec. G, Tab. 4). In terms of memory consumption, our approach requires less RAM and GPU memory than most alternatives. A detailed analysis is provided in Supp. Sec. G. Overall, our method is lightweight and practical, making it well-suited for zero-shot detection.

6. Conclusion

We introduced a novel conditional likelihood approach for zero-shot detection of generated images, leveraging CLIP embeddings and a whitening-based likelihood approximation conditioned on real images. Unlike existing methods, our approach naturally adapts to domain-specific scenarios, where others often underperform. Through extensive experiments on a large-scale dataset of over 200K real and generated images, we showed that our method outperforms prior zero-shot techniques in the general detection task. We further validated its adaptability on three challenging domains: artistic images, damaged car images and invoice images.

To support domain-specific evaluation, we presented two new synthetic datasets: over 6K damaged car images generated using five different models, and 3K invoice images generated using a single high-quality model. Our method is also efficient and lightweight, achieving fast inference and low memory usage. It is robust to input perturbations, parameter choices, and representative set variations. These findings highlight the promise of likelihood-based zero-shot detection and suggest that conditional likelihood estimation may serve as a foundation for broader tasks in computer vision such as out-of-distribution detection, and domain-adaptive representation learning.

Acknowledgements

We would like to acknowledge support by the Israel Science Foundation (Grant 1472/23) and by the Ministry of Innovation, Science and Technology (Grants No. 5074/22, 8801/25). We thank Shani Weiss for her assistance with generating the synthetic datasets.

References

- [1] Theodore W Anderson and Donald A Darling. A test of goodness of fit. *Journal of the American statistical association*, 49(268):765–769, 1954. 3
- [2] Anonymous, Danbooru community, and Gwern Branwen. Danbooru2021: A large-scale crowdsourced and tagged anime illustration dataset. <https://gwern.net/danbooru2021>, 2022. 7
- [3] Srikar Appalaraju, Bhavan Jasani, Bhargava Urala Kota, Yusheng Xie, and R Manmatha. Docformer: End-to-end transformer for document understanding. In *Proceedings of the IEEE/CVF international conference on computer vision*, pages 993–1003, 2021. 7
- [4] Quentin Bammey. Synthbuster: Towards detection of diffusion model generated images. *IEEE Open Journal of Signal Processing*, 2023. 2
- [5] Samah S Baraheem and Tam V Nguyen. Ai vs. ai: Can ai detect ai-generated images? *Journal of Imaging*, 9(10):199, 2023. 1, 2
- [6] James Betker, Gabriel Goh, Li Jing, Tim Brooks, Jianfeng Wang, Linjie Li, Long Ouyang, Juntang Zhuang, Joyce Lee, Yufei Guo, et al. Improving image generation with better captions. *Computer Science*. <https://cdn.openai.com/papers/dall-e-3.pdf>, 2(3):8, 2023. 5, 6
- [7] Roy Betsler, Meir Yossef Levi, and Guy Gilboa. Whitened clip as a likelihood surrogate of images and captions. In *International Conference on Machine Learning*. PMLR, 2025. 2, 3, 6
- [8] Jordan J Bird and Ahmad Lotfi. Cifake: Image classification and explainable identification of ai-generated synthetic images. *IEEE Access*, 2024. 1, 2
- [9] Delyan Boychev and Radostin Cholakov. Imagenet: A multi-content benchmark for synthetic image detection. In *Workshop on Datasets and Evaluators of AI Safety*, 2025. 7
- [10] Andrew Brock, Jeff Donahue, and Karen Simonyan. Large scale gan training for high fidelity natural image synthesis. *arXiv preprint arXiv:1809.11096*, 2018. 5
- [11] Jonathan Brokman, Omer Hofman, Roman Vainshtein, Amit Giloni, Toshiya Shimizu, Inderjeet Singh, Oren Rachmil, Alon Zolfi, Asaf Shabtai, Yuki Unno, et al. Montrage: Monitoring training for attribution of generative diffusion models. In *European Conference on Computer Vision*, pages 1–17. Springer, 2024. 7
- [12] Jonathan Brokman, Amit Giloni, Omer Hofman, Roman Vainshtein, Hisashi Kojima, and Guy Gilboa. Manifold induced biases for zero-shot and few-shot detection of generated images. In *International Conference on Learning Representations*, 2025. 1, 2, 5, 6, 7
- [13] Sheng Cao, Chao-Yuan Wu, , and Philipp Krähenbühl. Lossless image compression through super-resolution. *arXiv preprint arXiv:2004.02872*, 2020. 6
- [14] Mathilde Caron, Hugo Touvron, Ishan Misra, Hervé Jégou, Julien Mairal, Piotr Bojanowski, and Armand Joulin. Emerging properties in self-supervised vision transformers. In *Proceedings of the IEEE/CVF International Conference on Computer Vision (ICCV)*, pages 9650–9660, 2021. 6
- [15] Jiakuan Chen, Jieteng Yao, and Li Niu. A single simple patch is all you need for ai-generated image detection. *arXiv preprint arXiv:2402.01123*, 2024. 2
- [16] Qifeng Chen and Vladlen Koltun. Photographic image synthesis with cascaded refinement networks. In *Proceedings of the IEEE international conference on computer vision*, pages 1511–1520, 2017. 5
- [17] Dario Cioni, Christos Tzelepis, Lorenzo Seidenari, and Ioannis Patras. Are clip features all you need for universal synthetic image origin attribution? *arXiv preprint arXiv:2408.09153*, 2024. 1, 2
- [18] Davide Cozzolino, Giovanni Poggi, Riccardo Corvi, Matthias Nießner, and Luisa Verdoliva. Raising the bar of ai-generated image detection with clip. In *Proceedings of the IEEE/CVF Conference on Computer Vision and Pattern Recognition*, pages 4356–4366, 2024. 2
- [19] Davide Cozzolino, Giovanni Poggi, Matthias Nießner, and Luisa Verdoliva. Zero-shot detection of ai-generated images. In *European Conference on Computer Vision*, pages 54–72. Springer, 2024. 1, 2, 5, 6, 7
- [20] Ralph D’agostino and Egon S Pearson. Tests for departure from normality. empirical results for the distributions of b^2 and \sqrt{b} . *Biometrika*, 60(3):613–622, 1973. 3
- [21] Jia Deng, Wei Dong, Richard Socher, Li-Jia Li, Kai Li, and Li Fei-Fei. Imagenet: A large-scale hierarchical image database. In *2009 IEEE conference on computer vision and pattern recognition*, pages 248–255. Ieee, 2009. 8
- [22] Timo I Denk and Christian Reisswig. Bertgrid: Contextualized embedding for 2d document representation and understanding. *arXiv preprint arXiv:1909.04948*, 2019. 7
- [23] Prafulla Dhariwal and Alexander Nichol. Diffusion models beat gans on image synthesis. *Advances in neural information processing systems*, 34:8780–8794, 2021. 1, 5
- [24] Omar Elharrouss, Noor Almaadeed, Somaya Al-Maadeed, and Younes Akbari. Image inpainting: A review. *Neural Processing Letters*, 51:2007–2028, 2020. 3
- [25] David C Epstein, Ishan Jain, Oliver Wang, and Richard Zhang. Online detection of ai-generated images. In *Proceedings of the IEEE/CVF International Conference on Computer Vision*, pages 382–392, 2023. 1, 2
- [26] Sicheng Gao, Xuhui Liu, Bohan Zeng, Sheng Xu, Yanjing Li, Xiaoyan Luo, Jianzhuang Liu, Xiantong Zhen, and Baochang Zhang. Implicit diffusion models for continuous super-resolution. In *Proceedings of the IEEE/CVF conference on computer vision and pattern recognition*, pages 10021–10030, 2023. 2
- [27] Leon A Gatys, Alexander S Ecker, and Matthias Bethge. Image style transfer using convolutional neural networks. In *Proceedings of the IEEE conference on computer vision and pattern recognition*, pages 2414–2423, 2016. 7

- [28] Stuart Geman and Donald Geman. Stochastic relaxation, gibbs distributions, and the bayesian restoration of images. *IEEE Transactions on pattern analysis and machine intelligence*, 6:721–741, 1984. 3
- [29] Ian Goodfellow, Jean Pouget-Abadie, Mehdi Mirza, Bing Xu, David Warde-Farley, Sherjil Ozair, Aaron Courville, and Yoshua Bengio. Generative adversarial networks. *Communications of the ACM*, 63(11):139–144, 2020. 3
- [30] Bhawna Goyal, Ayush Dogra, Sunil Agrawal, Balwinder Singh Sohi, and Apoorav Sharma. Image denoising review: From classical to state-of-the-art approaches. *Information fusion*, 55:220–244, 2020. 3
- [31] Shuyang Gu, Dong Chen, Jianmin Bao, Fang Wen, Bo Zhang, Dongdong Chen, Lu Yuan, and Baining Guo. Vector quantized diffusion model for text-to-image synthesis. In *Proceedings of the IEEE/CVF conference on computer vision and pattern recognition*, pages 10696–10706, 2022. 5
- [32] Md Jahid Hasan, Agustinus Nalwan, Kok-Leong Ong, Hamed Jahani, Yee Ling Boo, Kha Cong Nguyen, and Mahmudul Hasan. Groundingcardd: Text-guided multimodal phrase grounding for car damage detection. *IEEE Access*, 2024. 7
- [33] Zhiyuan He, Pin-Yu Chen, and Tsung-Yi Ho. Rigid: A training-free and model-agnostic framework for robust ai-generated image detection. *arXiv preprint arXiv:2405.20112*, 2024. 1, 2, 5, 6
- [34] Dan Hendrycks, Steven Basart, Norman Mu, Saurav Kadavath, Frank Wang, Evan Dorundo, Rahul Desai, Tyler Zhu, Samyak Parajuli, Mike Guo, et al. The many faces of robustness: A critical analysis of out-of-distribution generalization. In *Proceedings of the IEEE/CVF international conference on computer vision*, pages 8340–8349, 2021. 4
- [35] Jonathan Ho, Ajay Jain, and Pieter Abbeel. Denoising diffusion probabilistic models. *Advances in neural information processing systems*, 33:6840–6851, 2020. 2
- [36] Micah Hodosh, Peter Young, and Julia Hockenmaier. Framing image description as a ranking task: Data, models and evaluation metrics. *Journal of Artificial Intelligence Research*, 47:853–899, 2013. 8
- [37] Yongcheng Jing, Yezhou Yang, Zunlei Feng, Jingwen Ye, Yizhou Yu, and Mingli Song. Neural style transfer: A review. *IEEE transactions on visualization and computer graphics*, 26(11):3365–3385, 2019. 7
- [38] Tero Karras, Timo Aila, Samuli Laine, and Jaakko Lehtinen. Progressive growing of gans for improved quality, stability, and variation. *arXiv preprint arXiv:1710.10196*, 2017. 5
- [39] Tero Karras, Samuli Laine, and Timo Aila. A style-based generator architecture for generative adversarial networks. In *Proceedings of the IEEE/CVF conference on computer vision and pattern recognition*, pages 4401–4410, 2019. 5
- [40] Tero Karras, Samuli Laine, Miika Aittala, Janne Hellsten, Jaakko Lehtinen, and Timo Aila. Analyzing and improving the image quality of stylegan. In *Proceedings of the IEEE/CVF conference on computer vision and pattern recognition*, pages 8110–8119, 2020. 5
- [41] Tero Karras, Miika Aittala, Samuli Laine, Erik Härkönen, Janne Hellsten, Jaakko Lehtinen, and Timo Aila. Alias-free generative adversarial networks. *Advances in neural information processing systems*, 34:852–863, 2021. 6
- [42] Bahjat Kawar, Shiran Zada, Oran Lang, Omer Tov, Huiwen Chang, Tali Dekel, Inbar Mosseri, and Michal Irani. Imagic: Text-based real image editing with diffusion models. In *Proceedings of the IEEE/CVF Conference on Computer Vision and Pattern Recognition*, pages 6007–6017, 2023. 2
- [43] Meir Yossef Levi and Guy Gilboa. The double-ellipsoid geometry of clip. In *International Conference on Machine Learning*. PMLR, 2025. 3
- [44] Haoying Li, Yifan Yang, Meng Chang, Shiqi Chen, Huajun Feng, Zhihai Xu, Qi Li, and Yueting Chen. Srdiff: Single image super-resolution with diffusion probabilistic models. *Neurocomputing*, 479:47–59, 2022. 3
- [45] Victor Weixin Liang, Yuhui Zhang, Yongchan Kwon, Serena Yeung, and James Y Zou. Mind the gap: Understanding the modality gap in multi-modal contrastive representation learning. *Advances in Neural Information Processing Systems*, 35:17612–17625, 2022. 3
- [46] Furqanil Taqwa (Linaqruf). Animate xl 2.0: High-resolution anime image generation. Hugging Face, 2023. 6, 7
- [47] Fernando Martin-Rodriguez, Rocio Garcia-Mojon, and Monica Fernandez-Barciela. Detection of ai-created images using pixel-wise feature extraction and convolutional neural networks. *Sensors*, 23(22):9037, 2023. 2
- [48] Midjourney. Midjourney: An independent research lab exploring new mediums of thought. <https://www.midjourney.com/>, 2024. Accessed: 2024-05-18. 5, 6
- [49] MindSpore. Wukong: A Pre-trained Model for Chinese Text-to-Image Generation. <https://xihe.mindspore.cn/modelzoo/wukong>, 2024. Accessed: 2024-05-18. 5
- [50] Ron Mokady, Amir Hertz, and Amit H Bermano. Clipcap: Clip prefix for image captioning. *arXiv preprint arXiv:2111.09734*, 2021. 2
- [51] Alex Nichol, Prafulla Dhariwal, Aditya Ramesh, Pranav Shyam, Pamela Mishkin, Bob McGrew, Ilya Sutskever, and Mark Chen. Glide: Towards photorealistic image generation and editing with text-guided diffusion models. *arXiv preprint arXiv:2112.10741*, 2021. 5
- [52] Utkarsh Ojha, Yuheng Li, and Yong Jae Lee. Towards universal fake image detectors that generalize across generative models. In *Proceedings of the IEEE/CVF Conference on Computer Vision and Pattern Recognition*, pages 24480–24489, 2023. 2, 6
- [53] OpenAI. GPT-Image-1: A multimodal image-generation model. <https://platform.openai.com/docs/models/gpt-image-1>, 2025. Released Apr 2025. 6, 7
- [54] Teerapong Panboonyuen, Naphat Nithisopa, Panin Pienroj, Laphonchai Jirachuphun, Chaiwasut Watthanasirikrit, and Naruepon Pornwiriyaikul. Mars: Mask attention refinement with sequential quadtree nodes for car damage instance segmentation. In *International Conference on Image Analysis and Processing*, pages 28–38. Springer, 2023. 7

- [55] Taesung Park, Ming-Yu Liu, Ting-Chun Wang, and Jun-Yan Zhu. Semantic image synthesis with spatially-adaptive normalization. In *Proceedings of the IEEE/CVF conference on computer vision and pattern recognition*, pages 2337–2346, 2019. 5
- [56] Kalpesh Patil, Mandar Kulkarni, Anand Sriraman, and Shirish Karande. Deep learning based car damage classification. In *2017 16th IEEE international conference on machine learning and applications (ICMLA)*, pages 50–54. IEEE, 2017. 7
- [57] Dustin Podell, Zion English, Kyle Lacey, Andreas Blattmann, Tim Dockhorn, Jonas Müller, Joe Penna, and Robin Rombach. Sdxl: Improving latent diffusion models for high-resolution image synthesis. *arXiv preprint arXiv:2307.01952*, 2023. 1, 6
- [58] Politico. Ai photography is here. so is the fight against disinformation. <https://www.politico.eu/article/ai-photography-machine-learning-technology-disinformation-midjourney-dall-e3-stable-diffusion/>, 2023. Accessed: 2025-03-01. 1
- [59] Tong Qiao, Hang Shao, Shichuang Xie, and Ran Shi. Unsupervised generative fake image detector. *IEEE Transactions on Circuits and Systems for Video Technology*, 2024. 1, 2
- [60] Alec Radford, Jong Wook Kim, Chris Hallacy, Aditya Ramesh, Gabriel Goh, Sandhini Agarwal, Girish Sastry, Amanda Askell, Pamela Mishkin, Jack Clark, et al. Learning transferable visual models from natural language supervision. In *International conference on machine learning*, pages 8748–8763. PMLR, 2021. 2, 3, 4, 5
- [61] Aditya Ramesh, Prafulla Dhariwal, Alex Nichol, Casey Chu, and Mark Chen. Hierarchical text-conditional image generation with clip latents. *arXiv preprint arXiv:2204.06125*, 1(2):3, 2022. 6, 7
- [62] Anton Razhigaev, Arseniy Shakhmatov, Anastasia Maltseva, Vladimir Arkhipkin, Igor Pavlov, Ilya Ryabov, Angelina Kuts, Alexander Panchenko, Andrey Kuznetsov, and Denis Dimitrov. Kandinsky: an improved text-to-image synthesis with image prior and latent diffusion. *arXiv preprint arXiv:2310.03502*, 2023. 6
- [63] Jonas Ricker, Denis Lukovnikov, and Asja Fischer. Aeroblade: Training-free detection of latent diffusion images using autoencoder reconstruction error. In *Proceedings of the IEEE/CVF Conference on Computer Vision and Pattern Recognition*, pages 9130–9140, 2024. 1, 2, 5, 6
- [64] Robin Rombach, Andreas Blattmann, Dominik Lorenz, Patrick Esser, and Björn Ommer. High-resolution image synthesis with latent diffusion models. In *Proceedings of the IEEE/CVF conference on computer vision and pattern recognition*, pages 10684–10695, 2022. 5, 6
- [65] Nikunj Saunshi, Orestis Plevrakis, Sanjeev Arora, Mikhail Khodak, and Hrishikesh Khandeparkar. A theoretical analysis of contrastive unsupervised representation learning. In *International Conference on Machine Learning*, pages 5628–5637. PMLR, 2019. 3
- [66] Christoph Schuhmann, Richard Vencu, Romain Beaumont, Robert Kaczmarczyk, Clayton Mullis, Aarush Katta, Theo Coombes, Jenia Jitsev, and Aran Komatsuzaki. Laion-400m: Open dataset of clip-filtered 400 million image-text pairs. *arXiv preprint arXiv:2111.02114*, 2021. 6
- [67] Zeyang Sha, Zheng Li, Ning Yu, and Yang Zhang. De-fake: Detection and attribution of fake images generated by text-to-image generation models. In *Proceedings of the 2023 ACM SIGSAC Conference on Computer and Communications Security*, pages 3418–3432, 2023. 2
- [68] Jiaming Song, Chenlin Meng, and Stefano Ermon. Denoising diffusion implicit models. *arXiv preprint arXiv:2010.02502*, 2020. 3
- [69] Chuangchuang Tan, Ping Liu, RenShuai Tao, Huan Liu, Yao Zhao, Baoyuan Wu, and Yunchao Wei. Data-independent operator: A training-free artifact representation extractor for generalizable deepfake detection. *arXiv preprint arXiv:2403.06803*, 2024. 2
- [70] Chunwei Tian, Lunke Fei, Wenxian Zheng, Yong Xu, Wangmeng Zuo, and Chia-Wen Lin. Deep learning on image denoising: An overview. *Neural Networks*, 131:251–275, 2020. 3
- [71] The Verge. That ai pope image is a fake—and an early glimpse of a new reality. <https://www.theverge.com/2023/3/27/23657927/ai-pope-image-fake-midjourney-computer-generated-aesthetic>, 2023. Accessed: 2025-03-01. 1
- [72] Sheng-Yu Wang, Oliver Wang, Richard Zhang, Andrew Owens, and Alexei A Efros. Cnn-generated images are surprisingly easy to spot... for now. In *Proceedings of the IEEE/CVF conference on computer vision and pattern recognition*, pages 8695–8704, 2020. 2, 6, 8
- [73] Xinkuang Wang, Wenjing Li, and Zhongcheng Wu. Cardd: A new dataset for vision-based car damage detection. *IEEE Transactions on Intelligent Transportation Systems*, 24(7):7202–7214, 2023. 7
- [74] Zhendong Wang, Jianmin Bao, Wengang Zhou, Weilun Wang, Hezhen Hu, Hong Chen, and Houqiang Li. Dire for diffusion-generated image detection. In *Proceedings of the IEEE/CVF International Conference on Computer Vision*, pages 22445–22455, 2023. 2
- [75] Zhizhong Wang, Lei Zhao, and Wei Xing. Stylediffusion: Controllable disentangled style transfer via diffusion models. In *Proceedings of the IEEE/CVF International Conference on Computer Vision*, pages 7677–7689, 2023. 7
- [76] wiF0n. invoiceXpert: A curated dataset of invoice images. <https://huggingface.co/datasets/wiF0n/invoiceXpert>, 2025. Accessed June 2025; license: CC-BY-NC-4.0. 7
- [77] WikiArt. Wikiart - visual art encyclopedia, 2024. 7
- [78] Junchao Wu, Shu Yang, Runzhe Zhan, Yulin Yuan, Lidia Sam Chao, and Derek Fai Wong. A survey on llm-generated text detection: Necessity, methods, and future directions. *Computational Linguistics*, pages 1–66, 2025. 2
- [79] Yiheng Xu, Minghao Li, Lei Cui, Shaohan Huang, Furu Wei, and Ming Zhou. Layoutlm: Pre-training of text and layout for document image understanding. In *Proceedings of the 26th ACM SIGKDD international conference on knowledge discovery & data mining*, pages 1192–1200, 2020. 7

- [80] Jiahui Yu, Zhe Lin, Jimei Yang, Xiaohui Shen, Xin Lu, and Thomas S Huang. Generative image inpainting with contextual attention. In *Proceedings of the IEEE conference on computer vision and pattern recognition*, pages 5505–5514, 2018. [3](#)
- [81] Mingxu Zhang, Hongxia Wang, Peisong He, Asad Malik, and Hanqing Liu. Exposing unseen gan-generated image using unsupervised domain adaptation. *Knowledge-Based Systems*, 257:109905, 2022. [2](#)
- [82] Mingxu Zhang, Hongxia Wang, Peisong He, Asad Malik, and Hanqing Liu. Improving gan-generated image detection generalization using unsupervised domain adaptation. In *2022 IEEE International Conference on Multimedia and Expo (ICME)*, pages 1–6. IEEE, 2022. [2](#)
- [83] Nan Zhong, Yiran Xu, Zhenxing Qian, and Xinpeng Zhang. Rich and poor texture contrast: A simple yet effective approach for ai-generated image detection. *arXiv preprint arXiv:2311.12397*, 2023. [2](#)
- [84] Jun-Yan Zhu, Taesung Park, Phillip Isola, and Alexei A Efros. Unpaired image-to-image translation using cycle-consistent adversarial networks. In *Proceedings of the IEEE international conference on computer vision*, pages 2223–2232, 2017. [5](#)
- [85] Mingjian Zhu, Hanting Chen, Qiangyu Yan, Xudong Huang, Guanyu Lin, Wei Li, Zhijun Tu, Hailin Hu, Jie Hu, and Yunhe Wang. Genimage: A million-scale benchmark for detecting ai-generated image, 2023. [6](#)
- [86] Daniel Zoran and Yair Weiss. From learning models of natural image patches to whole image restoration. In *2011 international conference on computer vision*, pages 479–486. IEEE, 2011. [3](#)